Nano Energy 132 (2024) 110381

Contents lists available at ScienceDirect

Nano Energy

journal homepage: www.elsevier.com/locate/nanoen

Boosting self-powered wearable thermoelectric generator with solar absorber and radiative cooler

Shuai Zhang [a,b,c,1], Zekun Liu [a,b,d,1], Zhenhua Wu [e,*], Zhengtong Yao [b], Wenbing Zhang [f], Yongwei Zhang [a], Zhihao Guan [b], Hengxin Lin [g], Haoge Cheng [h], Erzhen Mu [i], Jianwen Zeng [j], Chaochao Dun [k,*], Xiaotian Zhang [d,*], Johnny C. Ho [c], Zhiyu Hu [b,*]

[a] Department of Micro/Nano Electronics, School of Electronic Information and Electrical Engineering, Shanghai Jiao Tong University, Shanghai 200240, China
[b] Institute of NanoMicroEnergy, Zhangjiang Institute for Advanced Study, Shanghai Jiao Tong University, Shanghai 200240, China
[c] Department of Materials Science and Engineering, City University of Hong Kong, Kowloon, Hong Kong SAR 999077, China
[d] School of Mechanical and Power Engineering, East China University of Science and Technology, Shanghai 200237, China
[e] School of Mechanical Engineering, Shanghai Jiao Tong University, Shanghai 200240, China
[f] Institute of Engineering Thermophysics, School of Mechanical Engineering, Shanghai Jiao Tong University, Shanghai 200240, China
[g] State Key Laboratory of Functional Materials for Informatics, Shanghai Institute of Microsystem and Information Technology, Chinese Academy of Sciences, Shanghai 200050, China
[h] Qingdao Innovation and Development Center, Harbin Engineering University, Qingdao 266000, China
[i] School of Materials Science and Engineering, Henan Polytechnic University, Jiaozuo 454000, China
[j] School of Electronic Information, Wuhan University, Wuhan 430072, China
[k] The Molecular Foundry, Lawrence Berkeley National Laboratory, Berkeley, CA 94720, USA

ARTICLE INFO

Keywords:
Photothermal regulation
Radiative cooling
Selective solar absorber
Thermoelectric effect
Self-powered devices

ABSTRACT

The electrical output of wearable thermoelectric generators (wTEGs) has traditionally been constrained by small temperature differentials when powering microelectronics. In this study, we innovatively combine photothermal and radiative cooling mechanisms within a single wTEGs system, enabling substantial, uninterrupted power generation. Specifically, we designed a multilayer selective solar absorber (m-SSA) composed of flexible dielectric-metal stacks. This absorber demonstrates exceptional solar absorption efficiency of 93 % and significantly low thermal emissivity of 10 %. In practical outdoor conditions, it achieves a temperature increase of up to 108 °C under solar irradiation. Concurrently, we developed a flexible hierarchically porous radiative cooler (HP-RC), which reflects 96 % of solar energy and emits 97 % of thermal energy, achieving a cooling differential of up to 10 °C, even at ambient temperatures of 42 °C. Integration of the m-SSA and HP-RC with wTEGs allows for the simultaneous harvesting of heat from solar, cold space, and earth (robots or human body). This novel energy capture mechanism yielded a notable power density of 198 mW/m^2 for human body and 52 mW/m^2 for steel robots in outdoor wearable applications. This significant advancement promotes the field toward high-performance, integrated green power technologies and holds promise for next-generation wearable self-powered devices.

1. Introduction

The Earth exists in a state of dynamic equilibrium, influenced by the dual forces of solar heat and the cold void of space (Figure S1-S2). This perpetual interaction between the sun's relentless energy input and Earth's heat dissipation into space drives myriad natural phenomena and ecological processes. For instance, photosynthesis enables plants to transform solar energy into chemical energy. Simultaneously, the onset of colder seasons triggers frost formation on vegetation, illustrating the natural cycles of heating and cooling. These processes underscore the symbiotic relationship between life and its environment and inspire the development of tailored thermal management technologies that harness energy from both solar and space-derived sources. Recent advancements in technology and a deeper understanding of these natural mechanisms

* Corresponding authors.
E-mail addresses: wuzhenhua@sjtu.edu.cn (Z. Wu), cdun@lbl.gov (C. Dun), xiaotianzhang@sjtu.edu.cn (X. Zhang), zhiyuhu@sjtu.edu.cn (Z. Hu).
[1] These authors contributed equally to this work

https://doi.org/10.1016/j.nanoen.2024.110381
Received 25 September 2024; Received in revised form 16 October 2024; Accepted 16 October 2024
Available online 18 October 2024

have spotlighted the photothermal and radiative cooling effects as potential strategies for exploiting solar thermal energy and space chill, respectively [1]. The photothermal effect leverages solar radiation, predominantly spanning 0.3–2.5 μm, to maximize energy absorption and minimize thermal losses, facilitating effective self-heating. Conversely, the radiative cooling effect aims to minimize solar absorption while maximizing emission in the mid-infrared range, notably between 7 ~14 μm, where atmospheric transparency is highest. This approach enhances self-cooling by allowing terrestrial objects to effectively radiate heat back into space [2,3].

Thermoelectric generators can achieve solid-state energy conversion between heat and electricity through the Seebeck effect[4]. With the development of materials design (such as BiTe alloys, organic composites, GeTe and Cu_2X) and structural engineering (such as vertical, lateral, hybrid, inclined, annular and radial structures.) strategies, thermoelectric generators have potential application scenarios in the field of low-grade energy harvesting[4,5]. Wearable thermoelectric generators (wTEGs) have emerged as a sustainable power source by leveraging the stable temperature of the human body[6,7]. However, the small temperature difference between the human body and its surrounding environment limits the electricity generated, posing a challenge for powering microelectronic devices that typically require μWs to mWs of power[8,9]. To address this limitation, researchers have explored various heatsinks to increase the temperature difference across wTEGs, including convection, evaporation, and phase transition methods. For instance, Hu et al. enhanced air heat transfer by increasing surface wind speed, enabling the output of 456 mW/m^2 generated by wTEGs at a wind speed of 3 m/s to power temperature and humidity sensors via boost circuits [10]. An evaporative heatsink was devised for wTEG, resulting in a remarkable 48 % increase in output performance compared to natural convection[11]. This design facilitated battery-free, wireless monitoring of biochemical and physiological indicators, fully powered by the human body. Zhu et al. developed phase-change inorganics as cooling media for wTEGs, boosting output to 350 mW/m^2 and sustaining performance for 1.5 hours under static conditions[12]. Nevertheless, most of the solutions often entail increased volume, weight, additional energy consumption, restricted working conditions, and shorter lifespan, which are not conducive to the development of portable self-powered systems.

Recent advancements in integrated generators employing a solar absorber (SA) and/or radiative cooler (RC) in wTEGs can significantly improve temperature difference, thus boosting electricity generation [13–20]. The photothermal effect utilizes absorbed sunlight to facilitate self-heating. Typically, the SA is positioned atop vertical TEGs or one side of planar TEGs, creating temperature gradients between the SA (acting as the hot end) and the human body (acting as the cold end) [13–15]. The solar heating capacity of a SA is intricately linked to the characteristics of sunlight absorption and thermal radiation, which respectively represent the harvested energy and the lost energy [21]. Currently, broadband SA, encompassing carbon materials, polymer materials, and metal materials, have attracted widespread interest [22–25]. However, their strong thermal emission capabilities diminish the utilization of solar energy and weaken their impact on TEG output. Conversely, the radiative cooling effect achieves self-cooling by enhancing thermal emission in the mid-infrared range [26,27]. Leveraging the atmospheric transparent window, objects on Earth's surface radiate heat into cold space, effectively reducing their surface temperatures [28,29]. Incorporating an RC, also known as a thermal emitter, atop wTEG could further amplify temperature gradients and output performance through thermal management [16–20]. Here, the RC functions as the cold end, while the human body serves as the hot end. Unfortunately, due to the undesired solar heating effect, the radiative cooling mechanism is nearly ineffective during the daytime. Consequently, achieving dual-band synergistic regulation, characterized by low solar absorption and high mid-infrared emission, is crucial for attaining all-day self-cooling [3,28,30]. This necessitates the interdisciplinary integration of materials science, nanooptics, and thermodynamics.

Integrating SA or RC into wTEG presents a promising avenue for improving efficiency, and advancing the development of sustainable energy generation solutions[13,14,31]. Recently, the simultaneous integration SA and RC into TEGs has emerged[32–36]. We have previously developed sandwich-structured generators that continuously capture energy from both the sun and cold space, creating a temperature gradient across the vertical TEG for power generation[32]. Han et al. introduced a flexible design with zebra stripe-like patterns, combining RC and SA for all-day thermal energy harvesting and significant in-plane thermal gradient for thermoelectric generation[37]. Chen et al. devised a flexible 3D Janus helical ribbon architecture for efficient thermal management on both the cold and hot sides, achieving higher temperature gradients and all-day electricity generation[31]. These advancements offer valuable insights into simultaneously harnessing thermal energy from both the sun and cold space for power generation[13,14]. Nevertheless, utilizing multiple heat sources from the sun, cold space, and human body, and optimizing device structures to achieve significant output performance for wearable applications through thermal management still requires further exploration, with insufficient theoretical analysis and experimental validation.

The integration challenges of such systems, including the need for maintaining sufficient temperature differentials in wearable applications, are nontrivial. In this work, we have engineered high-performance selective SA by accurately designing the optical thickness of multi-layer thin films. These films show high solar absorption (93 %) and low thermal emissivity (10 %), which improve the ability to capture and convert solar energy, reduce thermal radiation losses, and be heated to 108 °C under outdoor solar irradiation. In addition, we have prepared hierarchically porous films with randomly embedded microspheres/nanoparticles for all-day radiative cooling. Benefiting from the regulatory effect of porous/multi-interface structure on the propagation path of electromagnetic waves, this RC exhibits high solar reflection (96 %) and infrared emission (97 %), which can reduce the influence of solar heating and improve its own thermal emission ability. In particular, it shows a cooling effect of 6–10 °C outdoors throughout the day. Finally, we designed an annular flexible thermoelectric generator and integrated it with a SA and RC to form a wTEGs, which could capture heat from the sun, cold space, and the human body. Through structural optimization and heat flow management, this self-powered generator achieves a power density of 198 mW/m^2 in real-world outdoor wearable scenes and provides a robust solution for powering wearable electronic devices.

2. Results and discussions

2.1. Flexible multilayer selective solar absorber

Although no naturally ideal SA exists, strategic manipulation of optical properties has enabled the design of high-performance SA. A notable example is the dielectric-metal periodic multilayer structure. This structure typically consists of a bottom metal infrared reflection layer, a dielectric layer with a low extinction coefficient, a semitransparent metal layer, and a top anti-reflection layer[21,38]. By controlling the thickness of each layer, incident light undergoes multiple reflections between the infrared-reflective layer and the semitransparent metal layer. This minimizes interference and achieves spectrally selective absorption, leading to efficient photothermal conversion (Figure S3).

We present a novel dielectric-metal multilayer selective solar absorber (m-SSA), which consists of an anti-reflective layer (Al_2O_3), a metal layer (Cr), a dielectric layer (Al_2O_3), a bonding layer (Cr), and an infrared reflective layer (Ag) from top to bottom (Fig. 1**a** and Figure S4). This structure was fabricated using the magnetron sputtering method, and the influence of the Cr layers across the solar (0.3–2.5 μm) and infrared (2.5–16 μm) spectral ranges was investigated (Figure S5-S6).

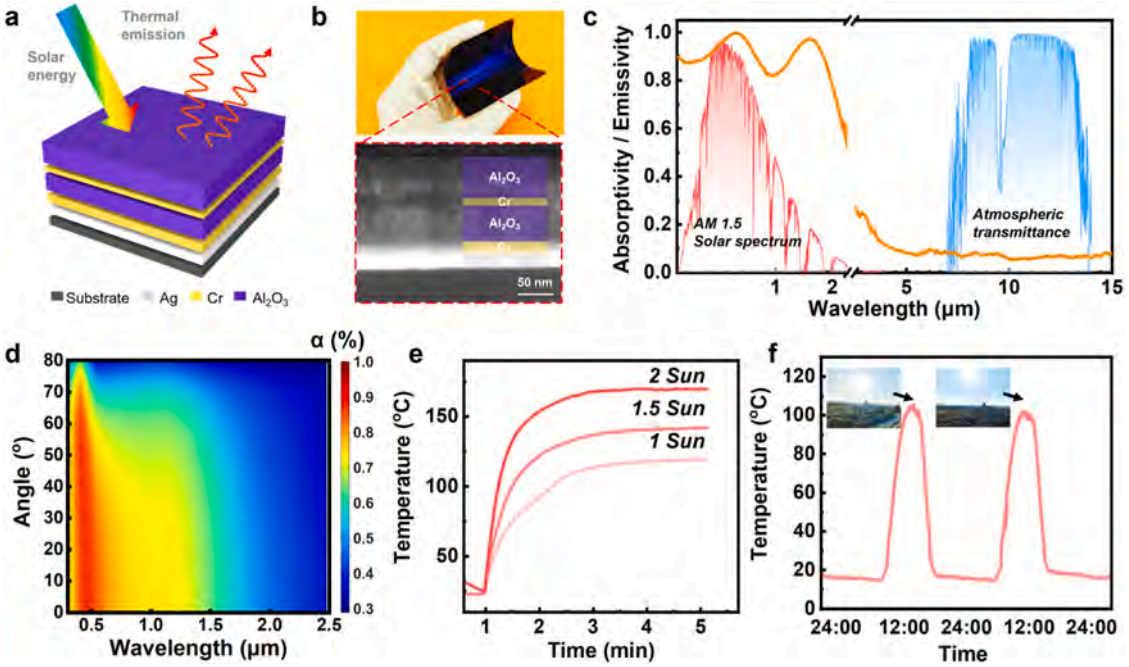

Fig. 1. Preparation process and performance of m-SSA. (a) Structural schematic diagram and basic principle; (b) Digital photo and cross-sectional SEM image; (c) The absorptance and emittance spectra of m-SSA, the inset red area represents the normalized AM1.5 solar spectrum and the blue area represents atmospheric transparency window; (d) The simulated solar absorptance at the different incidence angles; (e) Heating performance under different irradiation intensities; (f) Real-world outdoor photothermal performance.

Figure S7a and Table S1 reveal that the optimized thickness for the Cr metal layer in the solar spectrum is 10 nm, where m-SSA reaches an average solar absorptivity of 82 %. At this thickness, the infrared absorptivity stands at 12 %. Additionally, Cr is a commonly used bonding layer material in integrated circuit processes to improve the adhesion and stability between different media (Figure S4b). For the Cr bonding layer (Figure S7b and Table S2), increasing the thickness to approximately 15 nm maximizes the solar absorptivity at 93 %, while maintaining the infrared absorptivity at 10 %. Thus, the ideal thicknesses for achieving optimal absorptivity with m-SSA are 10 nm for the metal layer and 15 nm for the bonding layer. The m-SSA exhibits a smooth, flat surface with a distinguishable multilayer structure and a blue-purple appearance (Fig. 1**b and** Figure S8). It also demonstrates exceptional spectral selectivity, achieving high absorptivity in the solar spectrum and low absorptivity in the infrared range. At wavelengths of 0.6 μm and 1.5 μm, the absorptivity of m-SSA nears saturation, maintaining an average of approximately 93 % across the entire UV–vis–NIR spectrum, while its infrared absorptivity/emissivity remains low at around 10 %, as shown in Fig. 1**c**. Additionally, m-SSA efficiently absorbs omnidirectional solar radiation at incident angles from 1° to 80°, optimizing energy capture and conversion throughout the day (Fig. 1**d**). These results highlight the significant spectral selectivity of m-SSA and its potential as an effective solar absorber.

To assess its photothermal conversion properties, we also conducted heating tests under varying solar irradiances and evaluated its stability through multiple cycles (Fig. 1**e** and Figure S9a). The temperature rapidly escalated to 120 ℃ under standard solar irradiation (1000 W/m^2) and stabilized at 170 ℃ when the irradiance was doubled, demonstrating that increased irradiation enhances its heat absorption and generation capacity. Further tests under consistent irradiation confirmed the reproducibility and stability, with minimal temperature fluctuations, suggesting its viability for practical applications (Figure S9b). Additionally, we conducted a 48-hour continuous test in a natural setting on an unobstructed building roof (N 31°1′51″, E 121°26′26″). The outdoor tests highlighted the robust photothermal performance of our m-SSA, consistently reaching temperatures around 108 ℃ on clear days, thereby surpassing existing solutions without the need for concentrating optics (Fig. 1**f** and Figure S10).

2.2. *Flexible hierarchically porous radiative cooler*

Enhancing the reflection of sunlight is pivotal for improving daytime radiative cooling performance. Building on the strengths of the flexible m-SSA discussed above, we next integrate a flexible hierarchically porous RC to further enhance the temperature differential crucial for optimizing the power generation capabilities of wTEGs. Here, we used a solvent phase separation technique to develop a hierarchically porous RC (HP-RC) that achieves spectral selective regulation and efficient radiative cooling (Fig. 2**a** and Figure S11)[39]. By incorporating SiO_2 and $BaSO_4$ into the polymer precursor, and through solvent volatilization, we achieved a hierarchically porous structure embedded with nano/microparticles. This process is sensitive to temperature variations, which influence the phase separation and formation of porous structures (Figure S12).

The HP-RC displays a bright white appearance, as verified by the CIE chromaticity chart (Fig. 2**b** and Figure S13a). The surface is notably rough, maintaining an open pore structure that combines micrometer-scale pores within the polymer skeleton and nanoscale pores (Figs. 2**c**-2**d**). High-resolution SEM imaging shows that SiO_2 microspheres and $BaSO_4$ nanoparticles are randomly embedded within the porous skeleton, creating new interfaces at both the micrometer and nanometer scales (Fig. 2**e**). Pore size analysis reveals that the micropores predominantly measure around 11 μm, while the nanopores are generally less than 200 nm in diameter (Figs. 2**f**-2**g**). This arrangement leads to variations in the refractive index across the surface and interior of the film, enhancing the Mie scattering effect (Figure S13b).

The resulting multi-interface structure intensifies photon interactions, thus effectively modulating the spectral performance of the proposed HP-RC. Through Finite Difference Time Domain (FDTD) simulations, we confirmed that SiO_2 microspheres and $BaSO_4$ nanoparticles effectively redirect incident light and enhance scattering effects (Fig. 2**h**) [40,41]. Using COMSOL software, we observed that for

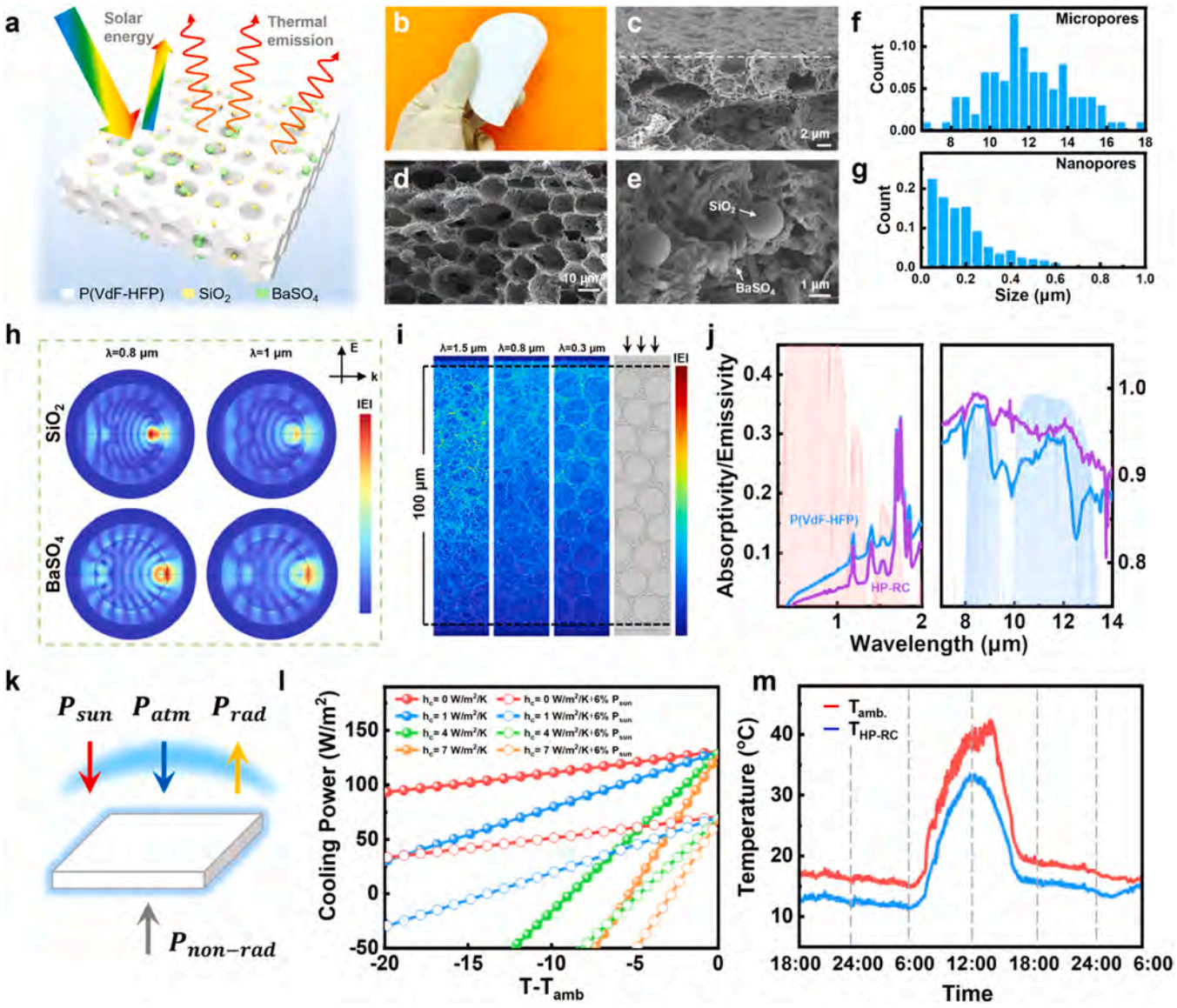

Fig. 2. Preparation process and performance of HP-RC. (a) Schematic illustrating the interaction between sunlight and thermal radiation of HP-RC; (b) Digital photo of HP-RC; SEM images of (c) the cross section at the interface; (d) The porous structure, and (e) the embedded particles. Size distributions of (f) micropores and (g) nanopores in HP-RC. (h) Electric field distributions of SiO_2 nanospheres and $BaSO_4$ microspheres by light with 0.8 μm and 1 μm wavelengths. (i) Propagated electrical field simulations of the HP-RC with the incident light wavelength of 0.3, 0.8, and 1.5 μm; (j) The absorptivity and emissivity of samples against the normalized AM 1.5 spectrum (the red area) and the atmospheric transparency window (the blue area); (k) Energy flow diagram of HP-RC; (l) Net cooling power in the nighttime (solid point) and daytime (hollow point); (m) Continuous outdoor temperature test.

short-wavelength light (0.3 μm), electromagnetic wave propagation is shallow within the HP-RC, primarily scattering at the interfaces of pores (air-polymer matrix) and filler boundaries. This significantly boosts the ability to scatter ultraviolet electromagnetic waves, thus reducing UV absorption within the film. As the wavelength increases, so does the depth of electromagnetic wave propagation within the film. Near the incident light side of the film, a pattern of randomly distributed high-intensity regions in the electric field was observed, demonstrating enhanced scattering capability for longer-wavelength light (Fig. 2**i**) [42–44]. Experimentally, the HP-RC film demonstrates a significant decrease in solar absorptivity compared to the standard P(VdF-HFP) film, particularly in the 1–2 μm range, indicating enhanced reflective properties in the long-wavelength (near-infrared) band (Fig. 2**j**). The average solar absorptivity of the composite film is below 6 %, a result of the inherent low absorptivity of the polymer combined with the Mie scattering effect from the fillers. In contrast, in the atmospheric transparent window, the standard P(VdF-HFP) film achieves an absorptivity of 92 %, largely due to its chemical composition and the enhancement of mid-infrared thermal emission from its micro-/nano-porous structure. With the inclusion of SiO_2 microspheres and $BaSO_4$ nanoparticles, the HP-RC film's absorptivity in this band significantly increases to 97 %.

In theory, the radiative cooling effect on the Earth's surface arises from the imbalance in radiative heat flow between sky-facing objects and cold space, with the atmosphere's transparent window serving as the primary channel for objects to radiate heat to cold space with minimal loss. As depicted in Fig. 2**k**, the thermal equilibrium state of an RC is influenced by solar radiation (P_{sun}), atmospheric radiation (P_{atm}), and non-radiative heat transfer from the environment ($P_{non-rad}$). Under these conditions, the cooling power (P_{cool}) of the radiative cooler can be expressed as[32]:

$$P_{cool}(T) = P_{rad}(T) - P_{atm}(T_{atm}) - P_{sun} - P_{non-rad}$$

Here, T represents the absolute temperature of the radiative cooler, while T_{atm} denotes the atmospheric temperature. P_{rad} signifies the power

radiated outward by a radiative cooler per unit area, serving as a measure of cooling capacity. Among these four fundamental heat flows, only P_{rad} represents output, whereas the other three types of power represent input. This indicates that the radiative cooler can solely dissipate heat through thermal radiation. As can be seen, our HP-RC demonstrates outstanding spectral selectivity, crucial for passive radiative cooling, and exhibits remarkable theoretical net cooling power both day and night (Fig. 2**l**). Its outdoor radiative cooling capacity was evaluated using the setup shown in Figure S14a, with Fig. 2**m** displaying the continuous measured temperature curve. At night, with ambient temperatures around 17 ℃, it radiates heat to cold space via mid-infrared electromagnetic waves, achieving a temperature reduction of 6 ℃. At noon, when solar radiation peaks at approximately 650 W/m^2 and ambient temperatures exceed 42 ℃, its high solar reflectivity significantly mitigates solar heating effects while continuing to emit heat to cold space, resulting in a 10 ℃ temperature drop. Furthermore, it maintains a cooling effect of 8 ℃ during cloudy days and 5 ℃ at night, underscoring its exceptional outdoor cooling capacity for practical applications (Figure S14b).

Besides, the current HP-RC showcases excellent mechanical properties, achieving robust flexibility and high durability, capable of enduring 25 % deformation and withstanding tensile forces over 4 N, as well as lifting weights exceeding 4 kg (Figure S15). It also exhibits superior hydrophobic properties, with water contact angles around 140° and similarly high angles for other liquids, although coffee shows slightly lower at 120° (Figure S16). HP-RC also demonstrates great potential for mass production, successfully implemented in large-scale thin films and adaptable for spray or brush applications on various substrates (Figure S17). Furthermore, it supports functional integration, such as spectral selective coatings for advanced thermal management. This scalable and cost-effective film presents an on-demand, zero-energy dual-mode approach to solar heating and radiative cooling, offering sustainable thermal energy harvesting or functional thermal management.

2.3. Self-powered thermoelectric generator integrating m-SSA and HP-RC

To maximize wTEGs performance by integrating m-SSA and HP-RC, we further engineered the homemade TEG (H-TEG) to achieve a higher filling factor and enhanced output compared to circular TEGs (C-TEG)

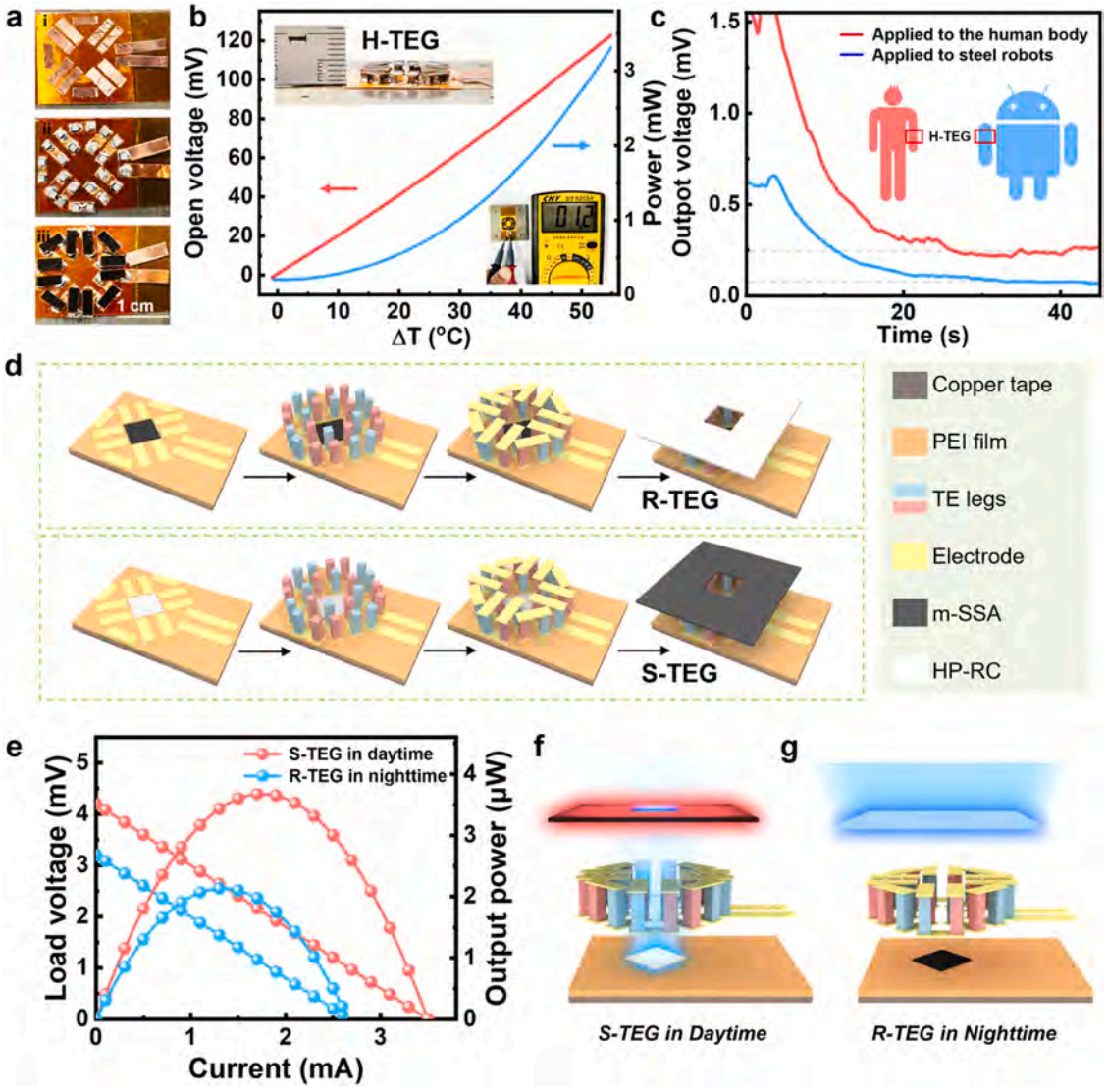

Fig. 3. Structure and properties of H-TEG, R-TEG and S-TEG. (a) The manufacturing process and (b) electrical output performance of H-TEG, the illustrations are physical images and resistance tests; (c) The output voltage when H-TEG is applied to the human body and steel robots. The manufacturing process of (d) R-TEG and S-TEG; (e) The output performance of S-TEG/R-TEG during different working periods. The working mechanism of (f) S-TEG during the daytime and (g) R-TEG during the nighttime.

[18]. The production process of the H-TEG mirrors that of the C-TEG, with significant differences in the arrangement and quantity of the thermoelectric legs. As illustrated in Figs. 3**a**-3**b**, the bottom electrodes of the H-TEG are densely packed along the edges and diagonals of the square substrate, connecting 12 pairs of P/N-type thermoelectric legs in series through welding. This configuration results in a filling factor of 26.6 % for the H-TEG, which is double that of the C-TEG. The open-circuit voltage of the H-TEG increases with rising temperature differentials: at a temperature differential of 10 °C, the voltage measures 22 mV, escalating to 110 mV at a differential of 50°C. When connected to an external load of 1.2 Ω which matches the internal resistance of H-TEG (Fig. 3**b**), the output power shows a corresponding increase with the temperature differential. At a 10 °C differential, the output power reaches 0.2 mW, and at an 80 °C differential, it surges to 7.1 mW.

Wearable self-powered devices, crucial for health monitoring and human-machine interaction, have seen increased demand with the rise of smart robots. Utilizing the human body and robots as heat sources, these devices, exemplified by our tested H-TEG, operate efficiently on both human body and steel-based robot skin, achieving steady-state voltages of 250 μV and 100 μV respectively (Fig. 3**c**). Due to the short

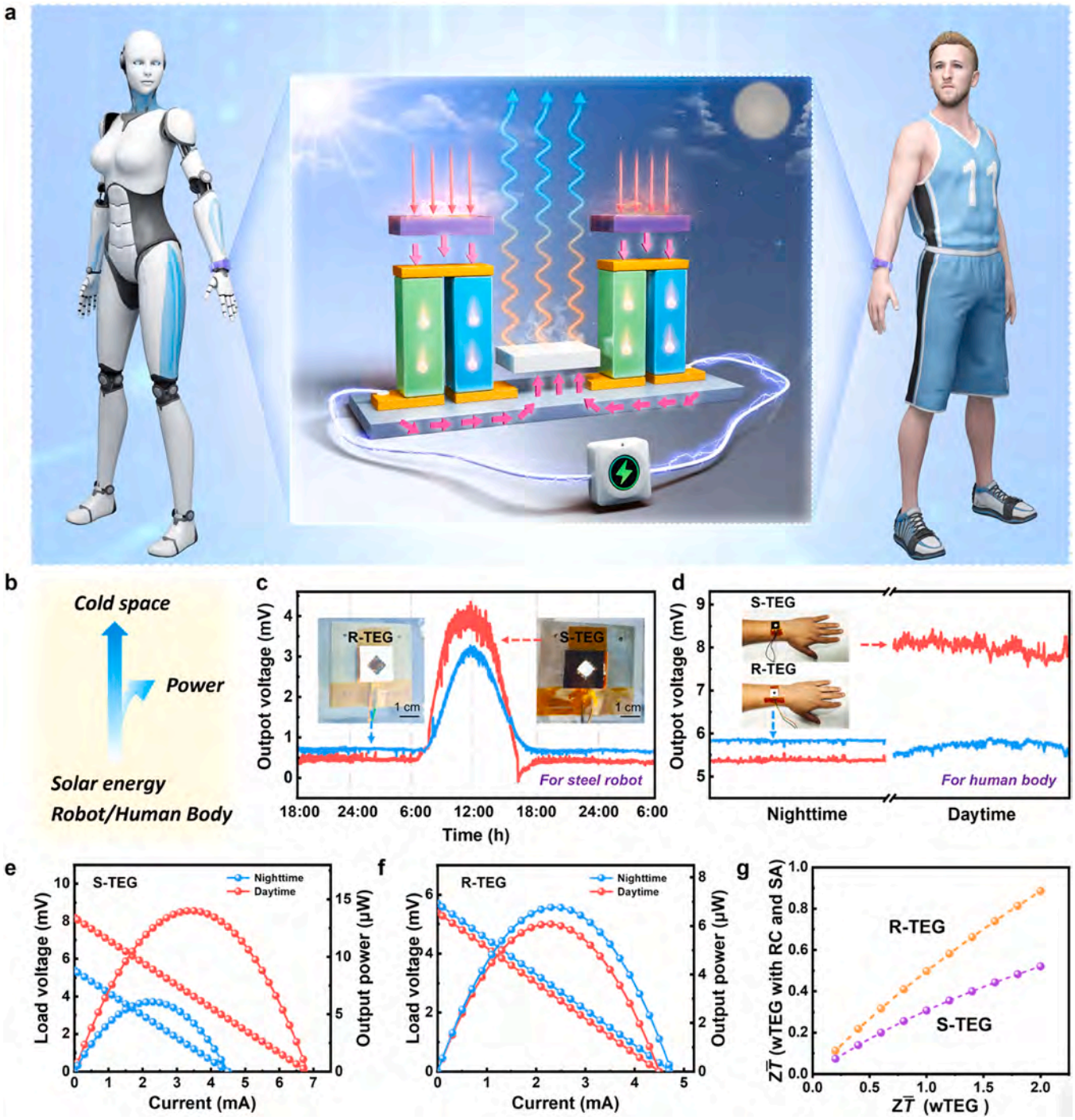

Fig. 4. Wearable self-powered generator. (a) Schematic diagram and (b) energy conversion process of wearable self-powered generators for robots and humans. Real-time output voltage for wearable self-powered generators (R-TEG and S-TEG) applied in (c) robots and (d) human body; The output performances of (e) S-TEG and (f) R-TEG in outdoor human wearable scenes during the nighttime and daytime measurements; (g) The effect of RC and SA on improving the performance of wTEG.

period of contact with the human body/steel robots, the temperature difference between the two ends of the generator gradually decreases to a stable state, so the output voltage also shows a trend of gradually decreasing to a stable state. Further enhancements include integrating solar absorbers, radiative coolers, and ultra-thin thermoelectric chips into a unified structure, boosting energy harvesting from both sunlight and the cold of space [18,32]. These experiments demonstrated significant potential, though optimization opportunities remain. Building upon the H-TEG, we propose a new integrated self-powered wearable generator. By combining the hollow sections at the top and middle of the thermoelectric device with an excellent solar absorber and a radiative cooler, this device can harvest energy from the human body/robots, sun, and cold space simultaneously (Figure S18). Fig. 3**d** presents two variants of the integrated generators based on H-TEG: 1) S-TEG, with the m-SSA positioned atop with an area ratio of m-SSA to HP-RC of 6:1, and 2) R-TEG, featuring the HP-RC at the top with an inverse area ratio of m-SSA to HP-RC of 1:6.

When S-TEG is exposed to clear sky and sunlight, it shows a peak power of 3.7 μW and an output power density of 52 mW/m^2 (Fig. 3**e**). This is attributed to S-TEG's enhanced solar energy absorption and conversion efficiency, leading to a higher temperature differential and subsequently a greater output voltage (Fig. 3**f**). For R-TEG with a larger HP-RC area at the top, it can radiate more heat into cold space at night, resulting in a considerable amount of heat flow to drive H-TEG operation (Fig. 3**g**). This integrated approach holds the promise of further improving output performance and represents a significant step forward in wearable energy generation technology.

2.4. Self-powered wearable thermoelectric generator for robots and human body

The device that simultaneously captures solar, space, and environmental energy (robots and human body) to achieve uninterrupted power generation provides a powerful solution for the next generation of green energy (Figs. 4**a**-4**b**) [45–48]. It is crucial to note that without integrating m-SSA and HP-RC, H-TEG is unable to produce a significant temperature difference/power output in practical applications (Fig. 3**c**). When equipped with m-SSA and HP-RC, H-TEG efficiently captures thermal energy from both the sun and cold space, facilitating continuous self-powered energy generation. To conduct quantitative evaluation and comparison, their performance was evaluated in an identical outdoor setting to assess their thermal energy harness capabilities and potential output disparities across different periods. For the application scenarios of robots (Fig. 4**c**), during the nighttime, R-TEG yields a voltage of 0.75 mV, while S-TEG and H-TEG (not equipped with HP-RC) record 0.5 mV and 100 μV respectively. This distinction stems from R-TEG's larger RC area, facilitating enhanced heat radiation into cold space and thus establishing a higher temperature difference. Conversely, during daylight hours, S-TEG demonstrates superior performance, generating an output voltage of 4.2 mV, surpassing the 3.1 mV produced by R-TEG under similar conditions. Over a four-day testing period (Figure S19), a consistent pattern emerges: S-TEG excels during the day, while R-TEG performs better at night. These insights shed light on the operational dynamics and potential applications of these integrated generators for robots.

Additionally, when in contact with human skin, the system harvests thermal energy from the sun, cold space, and the human body, in which humans act as the primary heat source (Fig. 4**a** and Fig. 4**d**). This interaction creates an additional temperature differential, thereby generating increased energy output: during nighttime when the m-SSA is inactive, the HP-RC plays a critical role in enhancing the temperature differential across the wearable thermoelectric generator TEG. In the R-TEG configuration, heat from the human body is transmitted vertically to the HP-RC, which then emits it into cold space via mid-infrared electromagnetic waves, maintaining continuous heat flow within the TEG and driving the directional movement of charge carriers. In contrast, the S-TEG configuration features a smaller HP-RC area closer to the human body, resulting in a more modest contribution to the temperature differential. As a result, during nighttime, the influence of the combined m-SSA and HP-RC on the output voltage in S-TEG is nearly negligible, with the temperature difference primarily due to the body's heat conducted along the TEG, dependent on the thermal conductivity and the length of the thermoelectric legs. During daytime operation, the m-SSA and HP-RC affect the output performance of the wearable TEGs differently. In R-TEG, the m-SSA within the hollow region efficiently captures sunlight and converts it to heat, which warms the adjacent area of the human body and rises along the thermoelectric legs together with the body-generated heat, establishing a stable temperature differential. Conversely, in S-TEG, the m-SSA positioned atop channels the absorbed solar energy downwards along the thermoelectric legs, heating the surface of the body. This heat merges with the human body heat that is transferred to the HP-RC located beneath, thereby creating a temperature gradient.

As shown in Fig. 4**d**, when in contact with human skin, R-TEG can produce a voltage of 5.7 mV at night, whereas S-TEG yields a voltage of 5.4 mV, underscoring the superior nighttime applicability of R-TEG for wearable self-power supply. Meanwhile, during the day, S-TEG can output a voltage of 8.2 mV, while R-TEG yields a voltage of 5.4 mV. This outcome underscores the superiority of S-TEG in the realm of daytime wearable self-generation. Observing the load voltage/output power-current curves depicted in Figs. 4**e**-4**f**, it becomes apparent that S-TEG can attain maximum output powers of 14.0 μW (198 mW/m^2) and 6.0 μW (86 mW/m^2) output power during daytime and nighttime, respectively. In comparison, R-TEG achieves up to 6.7 μW (95 mW/m^2) and 6.0 μW (86 mW/m^2) output power during the day and at night, respectively. When achieving comparable output performance, the combined effects of SA and RC in enhancing the temperature difference of wearable TEGs equate to an increase in the *ZT* value of thermoelectric devices (Fig. 4**g**). Generally, doubling the *ZT* value by improving thermoelectric properties alone is quite challenging. For S-TEG operating under daytime conditions, this enhancement corresponds to a fourfold increase in the *ZT* value of thermoelectric devices, while for R-TEG operating under nighttime conditions, it represents a 2.2-fold increase.

As shown in Fig. 5**a** and Table S3, the integrated self-powered generator developed in this study demonstrates competitive advantages, achieving a notable power density of 198 mW/m^2 for human body applications and 52 mW/m^2 for robot applications [10,16,18,34,49–51]. This generator can potentially power a wide range of microelectronic devices—from IoT devices and RFID tags to gas detectors and smartwatches—which typically require μW to mW levels of power for daily operations (Figs. 5**b**-5**c**) [13,14,52–54]. Such a capability enables these devices to operate without the need for frequent charging or battery replacements, enhancing user experience.

3. Conclusions

In sum, we developed a flexible, wearable, self-powered generator by integrating an m-SSA, a hierarchically porous HP-RC, and a flexible H-TEG. We refined the structural parameters of the m-SSA's dielectric-metal stacked structure, which includes an anti-reflective layer, metal layer, dielectric layer, bonding layer, and infrared reflective layer. The HP-RC, fabricated using the solvent phase separation method, achieved synergistic control of solar light absorption and mid-infrared thermal emission. This large-area film also features robust mechanical properties and hydrophobicity, enhancing its suitability for complex outdoor environments. Moreover, optimizing the geometric parameters and structure of the H-TEG significantly increased its filling factor to 26.6 %. Finally, the integration of m-SSA, HP-RC, and H-TEG led to the creation of two generators, R-TEG and S-TEG, each designed with distinct thermal management strategies to harness energy from the sun, cold space, and the human body (or robots). In outdoor wearable scenarios, S-TEG produced 198 mW/m^2 during the day and 86 mW/m^2 at night, while R-

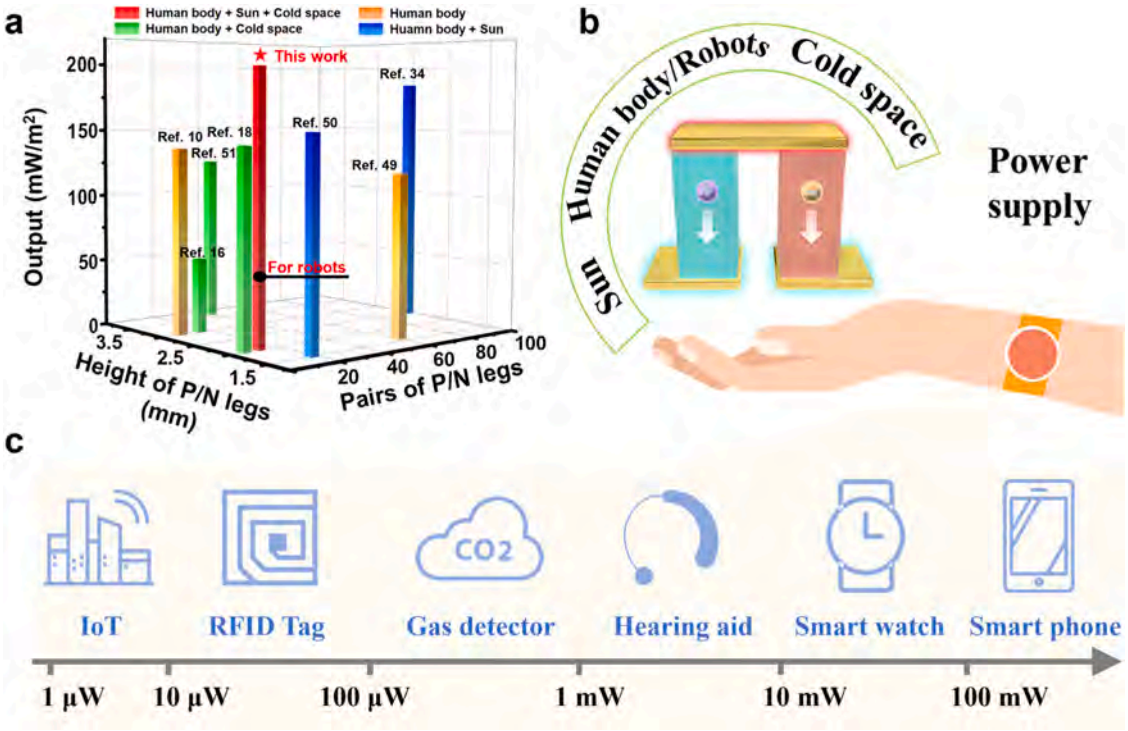

Fig. 5. Performance Comparison and Application Potential. (a) Comparison between geometric parameters and output performance; (b-c) Application scenario of the self-powered wearable thermoelectric generators.

TEG generated 95 mW/m^2 and 86 mW/m^2 respectively for the same periods. The application of this generator in steel robot also achieves a power density of 52 mW/m^2, demonstrating the potential for self-powering robots that can be worn over a large area.These results highlight the potential of our integrated generators for powering wearable electronics, improving device portability and autonomy, and advancing related technologies.

CRediT authorship contribution statement

Zhihao Guan: Validation, Investigation. **Hengxin Lin:** Validation, Investigation. **Haoge Cheng:** Investigation. **Erzhen Mu:** Methodology. **Jianwen Zeng:** Visualization. **Chaochao Dun:** Writing – review & editing, Investigation. **Shuai Zhang:** Writing – original draft, Visualization, Validation, Resources, Methodology, Investigation, Formal analysis, Data curation, Conceptualization. **Xiaotian Zhang:** Writing – review & editing, Supervision, Project administration, Funding acquisition. **Zekun Liu:** Validation, Resources, Methodology, Data curation. **Johnny C. Ho:** Writing – review & editing. **Zhenhua Wu:** Writing – review & editing, Supervision, Project administration, Funding acquisition, Data curation. **Zhiyu Hu:** Writing – review & editing, Supervision, Project administration, Conceptualization. **Zhengtong Yao:** Visualization, Methodology, Formal analysis. **Wenbing Zhang:** Validation, Software, Methodology. **Yongwei Zhang:** Visualization, Software, Methodology.

Declaration of Competing Interest

The authors declare that they have no known competing financial interests or personal relationships that could have appeared to influence the work reported in this paper.

Acknowledgments

S. Zhang and Z. Liu contributed equally to this work. We would like to thank Prof. Kasper Moth-Poulsen from Universitat Politècnica de Catalunya for his help in theoretical analysis and language polishing. The authors thank the National Natural Science Foundation of China (grant 62201345, 51776126, and 52202179), Education Department of Henan Province (22B470005), the Center of Advanced Electronic Materials and Devices (AEMD), and the Instrumental Analysis Center of Shanghai Jiao Tong University. The authors also thank Mr. Zhao from Shiyanjia Lab (www.shiyanjia.com) for the drawing schematic illustration.

Appendix A. Supporting information

Supplementary data associated with this article can be found in the online version at doi:10.1016/j.nanoen.2024.110381.

Data Availability

Data will be made available on request.

References

[1] L. Zhu, Tian, S. Jiang, L. Han, Y. Liang, Q. Li, S. Chen, Advances in photothermal regulation strategies: from efficient solar heating to daytime passive cooling, Chem. Soc. Rev. 52 (2023) 7389–7460, https://doi.org/10.1039/d3cs00500c.
[2] J. Ma, F. Zeng, X. Lin, Y. Wang, Y. Ma, X. Jia, J. Zhang, B. Liu, Y. Wang, H. Zhao, A photoluminescent hydrogen-bonded biomass aerogel for sustainable radiative cooling, Science 385 (2024) 68–74. ⟨https://www.science.org/doi/10.1126/science.adn5694⟩.
[3] C. Wang, H. Chen, F. Wang, Passive daytime radiative cooling materials toward real-world applications, Prog. Mater. Sci. 2024 (144) (2024) 101276, https://doi.org/10.1016/j.pmatsci.2024.101276.
[4] X.-L. Shi, L. Wang, W. Lyu, T. Cao, W. Chen, B. Hu, Z.-G. Chen, Advancing flexible thermoelectrics for integrated electronics, Chem. Soc. Rev. 53 (2024) 9254, https://doi.org/10.1039/D4CS00361F.
[5] T. Cao, X.L. Shi, J. Zou, Z.-G. Chen, Advances in conducting polymer-based thermoelectric materials and devices, Microstructures 1 (2021) 2021007, https://doi.org/10.20517/microstructures.2021.06.
[6] C. Hou, M. Zhu, Semiconductors flex thermoelectric power, Science 277 (2022) 6608. ⟨https://www.science.org/doi/10.1126/science.add7029⟩.
[7] W. Tang, Q. Sun, Z. Wang, Self-powered sensing in wearable electronics-a paradigm shift technology, Chem. Rev. 123 (2023) 12105–12134, https://doi.org/10.1021/acs.chemrev.3c00305.

[8] L. Qi, L. Kong, Y. Wang, J. Song, A. Azam, Z. Zhang, J. Yan, Recent progress in application-oriented self-powered microelectronics, Adv. Energy Mater. 13 (2023) 2302699, https://doi.org/10.1002/aenm.202302699.

[9] Y. Liu, L. Yin, W. Zhang, J. Wang, S. Hou, Z. Wu, Z. Zhang, C. Chen, X. Li, H. Ji, Q. Zhang, Z. Liu, F. Chao, A wearable real-time power supply with a Mg_3Bi_2-based thermoelectric module, Cell Rep. Phy. Sci. 2 (2021) 100412, https://doi.org/10.1016/j.xcrp.2021.100412.

[10] K. Hu, D. Yang, Y. Hui, H. Zhang, R. Song, Y. Liu, J. Wang, P. Wen, D. He, X. Liu, Y. Yan, X. Tang, Optimized thermal design for excellent wearable thermoelectric generator, J. Mater., Chem. A 10 (2022) 24985–24994, https://doi.org/10.1039/d2ta06966k.

[11] Z. An, Q. Fu, J. Lv, T. Zhou, Y. Wu, Y. Lu, G. Liu, Z. Shi, X. li, F. Zhang, Q. Liu, Body heat powered wirelessly wearable system for real-time physiological and biochemical monitoring, Adv. Funct. Mater. 33 (2023) 2303361, https://doi.org/10.1002/adfm.202303361.

[12] S. Zhu, L. Miao, Y. Peng, J. Gao, H. Lai, C. Liu, Y. Zhang, X. Zhang, Z. Chen, Y. Pei, Persistently self-powered wearable thermoelectric generator enabled by phase-change inorganics as the heat sink, Mater. Today Phy. 32 (2023) 101011, https://doi.org/10.1016/j.mtphys.2023.101011.

[13] S. Zhang, Z. Liu, X. Zhang, Z. Wu, Z.Y. Hu, Sustainable thermal energy harvest for generating electricity, Innovation 5 (2024) 100591, https://doi.org/10.1016/j.xinn.2024.100591.

[14] S. Zhang, Z. Wu, Z. Liu, Z. Hu, An emerging energy technology: Self-uninterrupted electricity power harvesting from the sun and cold space, Adv. Energy Mater. 13 (2023) 2300260, https://doi.org/10.1002/aenm.202300260.

[15] X. Zhang, T. Li, H. Ren, H. Peng, B. Shiu, Y. Wang, C. Lou, J. Lin, Dual-shell photothermoelectric textile based on a PPy photothermal layer for solar thermal energy harvesting, ACS Appl. Mater. Interfaces 12 (2020) 55072–55082, https://doi.org/10.1021/acsami.0c16401.

[16] Y. Liu, S. Hou, X. Wang, L. Yin, Z. Wu, X. Wang, J. Mao, J. Sui, X. Liu, Q. Zhang, Z. Liu, F. Cao, Passive radiative cooling enables improved performance in wearable thermoelectric generators, Small 18 (2022) 2106875, https://doi.org/10.1002/smll.202106875.

[17] H. Pan, D. Zhao, An improved model for performance predicting and optimization of wearable thermoelectric generators with radiative cooling, Energ. Convers. Manag. 284 (2023) 116981, https://doi.org/10.1016/j.enconman.2023.116981.

[18] S. Zhang, Z. Liu, W. Zhang, B. Zhao, Z. Wu, E. Mu, H. Lin, K. Zou, Y. Zhang, X. Zhang, Z. Hu, Multi-bioinspired flexible thermal emitters for all-day radiative cooling and wearable self-powered thermoelectric generation, Nano Energy 123 (2024) 109393, https://doi.org/10.1016/j.nanoen.2024.109393.

[19] Z. Wu, S. Zhang, Z. Liu, E. Mu, Z. Hu, Thermoelectric converter: Strategies from materials to device application, Nano Energy 91 (2022) 106692, https://doi.org/10.1016/j.nanoen.2021.106692.

[20] Z. Wu, Z. Hu, Perspective-Powerful micro/nano-scale heat engine: thermoelectric converter on chip, ECS Sens. 1 (2022) 023402, https://doi.org/10.1149/2754-2726/ac7534.

[21] C. He, Y. Li, Z. Zhou, B. Liu, X. Gao, High-entropy photothermal materials, Adv. Mater. 36 (2024) 2400920, https://doi.org/10.1002/adma.202400920.

[22] P. Cheng, D. Wang, P. Schaaf, A review on photothermal conversion of solar energy with nanomaterials and nanostructures: From fundamentals to applications, Adv. Sustain. Syst. 6 (2022) 2200115, https://doi.org/10.1002/adsu.202200115.

[23] X. Cui, Q. Ruan, X. Zhu, X. Xia, J. Hu, R. Fu, Y. Li, J. Wang, H. Xu, Photothermal nanomaterials: a powerful light-to-heat converter, Chem. Rev. 123 (2023) 6891–6952, https://doi.org/10.1021/acs.chemrev.3c00159.

[24] S. Zhang, Z. Wu, Z. Liu, Y. Lv, Z. Hu, Nanostructured broadband solar absorber for effective photothermal conversion and electricity generation, Energies 15 (2022) 1354, https://doi.org/10.3390/en15041354.

[25] J. Zhang, T. Tang, R. Yang, G. Wang, K.H. Ye, J. Shi, Photothermal effect and application of photothermal materials in photocatalysis and photoelectric catalysis, Microstructures 4 (2024) 2024008, https://doi.org/10.20517/microstructures.2023.51.

[26] M. Lee, G. Kim, Y. Jung, K.R. Pyun, J. Lee, B.W. Kim, S.H. Ko, Photonic structures in radiative cooling, Light Sci. Appl. 12 (2023) 134, https://doi.org/10.1038/s41377-023-01119-0.

[27] Y. Wang, H. Ji, B. Liu, P. Tang, Y. Chen, J. Huang, Y. Ou, J. Tao, Radiative cooling: structure design and application, J. Mater. Chem. A 12 (2024) 9962–9978, https://doi.org/10.1039/d4ta01158a.

[28] R. Liu, S. Wang, Z. Zhou, K. Zhang, G. Wang, C. Chen, Y. Long, Materials in radiative cooling technologies, Adv. Mater. (2024) 2401577, https://doi.org/10.1002/adma.202401577.

[29] S. Zhang, Z. Wu, Z. Liu, H. Lin, Z. Lin, J. Li, S. Kong, Z. Hu, Cost effective 24-h radiative cooler with multiphase interface enhanced solar scattering and thermal emission, Mater. Today Commun. 31 (2022) 103398, https://doi.org/10.1016/j.mtcomm.2022.103398.

[30] Z. Yan, H. Zhai, D. Fan, Q. Li, Biological optics, photonics and bioinspired radiative cooling, Prog. Mater. Sci. 144 (2024) 101291, https://doi.org/10.1016/j.pmatsci.2024.101291.

[31] C. Chen, B. Zhao, R. Wang, Z. He, J. Wang, M. Hu, X. Li, G. Pei, J. Liu, S. Yu, Janus helical ribbon structure of ordered nanowire films for flexible solar thermoelectric devices, Adv. Mater. 34 (2022) 2206364, https://doi.org/10.1002/adma.202206364.

[32] S. Zhang, Z. Wu, Z. Liu, E. Mu, Y. Liu, Y. Lv, T. Thundat, Z. Hu, Power generation on chips: Harvesting energy from the sun and cold space, Adv. Mater. Technol. 7 (2022) 2200478, https://doi.org/10.1002/admt.202200478.

[33] M. Feng, S. Lv, J. Deng, Y. Guo, Y. Wu, G. Shi, M. Zhang, An overview of environmental energy harvesting by thermoelectric generators, Renew. Sust. Energ. Rev. (2023), https://doi.org/10.1016/j.rser.2023.113723.

[34] Y. Jung, S. Jeong, J. Ahn, J. Lee, S.H. Ko, High efficiency breathable thermoelectric skin using multimode radiative cooling/solar heating assisted large thermal gradient, Small 20 (2024) 2304338, https://doi.org/10.1002/smll.202304338.

[35] M. Liao, D. Banerjee, T. Hallberg, C. Akerlind, M. Alam, Q. Zhang, H. Kariis, D. Zhao, M. Jonsson, Cellulose-based radiative cooling and solar heating powers ionic thermoelectrics, Adv. Sci. 10 (2023) 2206510, https://doi.org/10.1002/advs.202206510.

[36] X. Min, X. Wang, J. Li, N. Xu, X. Du, M. Zeng, W. Li, B. Zhu, J. Zhu, A smart thermal-gated bilayer membrane for temperature-adaptive radiative cooling and solar heating, Sci. Bull. 68 (2023) 2054–2062, https://doi.org/10.1016/j.scib.2023.08.003.

[37] W. Han, S. Heo, D. Kim, S. Yang, G. Ko, G. Lee, D. Kim, K. Rajaram, J. Lee, J. Shin, T. Jang, S. Han, H. Kang, J. Lim, D. Kim, S. Kim, Y. Song, S. Hwang, Zebra-inspired stretchable, biodegradable radiation modulator for all-day sustainable energy harvesters, Sci. Adv. 9 (2023), https://doi.org/10.1126/sciadv.adf5883.

[38] J. Ren, D. Liang, H. Liu, Y. Yang, A. Li, Y. Sun, C. Wang, High-temperature thermal stable solar selective absorbing coating based on the dielectric-metal-dielectric structure, Mater. Today Phys. 34 (2023) 101092, https://doi.org/10.1016/j.mtphys.2023.101092.

[39] J. Mandal, Y. Fu, A. Overvig, M. Jia, K. Sun, N. Shi, H. Zhou, X. Xiao, N. Yu, Y. Yang, Hierarchically porous polymer coatings for highly efficient passive daytime radiative cooling, Science 362 (2018) 315–318, https://doi.org/10.1126/science.aat9513.

[40] P. Li, A. Wang, J. Fan, Q. Kang, P. Jiang, H. Bao, X. Huang, Thermo-optically designed scalable photonic films with high thermal conductivity for subambient and above-ambient radiative cooling, Adv. Funct. Mater. 32 (2022) 2109542, https://doi.org/10.1002/adfm.202109542.

[41] C. Park, C. Park, S. Park, J. Lee, Y. Kim, Y. Yoo, Hybrid emitters with raspberry-like hollow SiO_2 spheres for passive daytime radiative cooling, Chem. Eng. J. 459 (2023) 141652, https://doi.org/10.1016/j.cej.2023.141652.

[42] M. Kang, G. Lee, J. Lee, M. Kim, Z. Yan, J. Jeong, K. Jang, Y. Song, Outdoor-useable, wireless/battery-free patch-type tissue oximeter with radiative cooling, Adv. Sci. 8 (2021) 2004885, https://doi.org/10.1002/advs.202004885.

[43] J. Li, Y. Fu, J. Zhou, K. Yao, X. Ma, S. Gao, Z. Wang, J. Dai, D. Lei, X. Yu, Ultrathin, soft, radiative cooling interfaces for advanced thermal management in skin electronics, Sci. Adv. 9 (2023), https://doi.org/10.1126/sciadv.adg1837.

[44] Y. Tian, X. Liu, Z. Wang, J. Li, Y. Mu, S. Zhou, F. Chen, M. Minus, G. Xiao, Y. Zheng, Subambient daytime cooling enabled by hierarchically architected all-inorganic metapaper with enhanced thermal dissipation, Nano Energy 96 (2022) 107085, https://doi.org/10.1016/j.nanoen.2022.107085.

[45] M. Yoo, K. Pyun, Y. Jung, M. Lee, J. Lee, S. Ko, Switchable radiative cooling and solar heating for sustainable thermal management, Nanophotonics 13 (2024) 543–561, https://doi.org/10.1515/nanoph-2023-0627.

[46] S. Zhou, P. Chen, C. Xiao, Y. Ge, H. Gao, Recent advances in dynamic dual mode systems for daytime radiative cooling and solar heating, RSC Adv. 13 (2023) 31738–31755, https://doi.org/10.1039/d3ra05506j.

[47] Y. Zhao, W. Jiang, S. Zhuo, B. Wu, P. Luo, W. Chen, M. Zheng, J. Hu, K. Zhang, Z. Wang, L. Liao, M. Zhuo, Stretchable photothermal membrane of NIR-II charge-transfer cocrystal for wearable solar thermoelectric power generation, Sci. Adv. 9 (2023), https://doi.org/10.1126/sciadv.adh8917.

[48] H. Zhang, Z. Wang, H. Li, M. Salla, Y. Song, S. Huang, S. Huang, X. Wang, K. Liu, G. Xu, J. Huang, C. Qu, Q. Wang, Continuous electricity generation from solar heat and darkness, Joule 7 (2023) 1515–1528, https://doi.org/10.1016/j.joule.2023.06.009.

[49] W. Fan, Z. An, F. Liu, Z. Gao, M. Zhang, C. Fu, T. Zhu, Q. Liu, X. Zhao, High-performance stretchable thermoelectric generator for self-powered wearable electronics, Adv. Sci. 10 (2023) e2206397, https://doi.org/10.1002/advs.202206397.

[50] M. Jeong, K. Kim, J. Kim, K. Choi, Operation of wearable thermoelectric generators using dual sources of heat and light, Adv. Sci. 9 (2022) 2104915, https://doi.org/10.1002/advs.202104915.

[51] S. Khan, J. Kim, K. Roh, G. Park, W. Kim, High power density of radiative-cooled compact thermoelectric generator based on body heat harvesting, Nano Energy 87 (2021) 106180,, https://doi.org/10.1016/j.nanoen.2021.106180.

[52] S. Wang, G. Zuo, J. Kim, H. Sirringhaus, progress of conjugated polymers as emerging thermoelectric materials, Prog. Polym. Sci. 129 (2022) 101548, https://doi.org/10.1016/j.progpolymsci.2022.101548.

[53] Y. Shi, X. Lü, Q. Xiang, J. Li, X. Shao, W. Bao, Stretchable thermoelectric generator for wearable power source and temperature detection applications, Energ. Conv. Manag. 253 (2022) 115167, https://doi.org/10.1016/j.enconman.2021.115167.

[54] J. Kim, S. Khan, P. Wu, S. Park, H. Park, C. Yu, W. Kim, Self-charging wearables for continuous health monitoring, Nano Energy 79 (2021) 105419, https://doi.org/10.1016/j.nanoen.2020.105419.

Shuai Zhang is a postdoctoral fellow in the Department of Materials Science and Engineering at the City University of Hong Kong. He received the Ph.D. degree from the Department of Micro/Nano Electronics, Shanghai Jiao Tong University in 2024. His research interests include micro-nano fabrication, photothermal manipulation, self-powered generators, and hydrogel-based sensors.

Zekun Liu is currently a lecturer at the School of Mechanical and Power Engineering, East China University of Science and Technology. He received his Ph. D. degree in Shanghai Jiao Tong University in 2024. His research interests include fabrication of MEMS thermoelectric devices, application of micro-TED in sensing, and efficient and comprehensive utilization of energy.

Zhenhua Wu received his PhD degree in the School of Electronic Information and Electrical Engineering at Shanghai Jiao Tong University in 2020 and then continued his postdoctoral research there from 2020 to 2023. Currently, he is a research scientist at Shanghai Jiao Tong University. His research interests include thermoelectric, memristor and nano/micro fabrication.

Chaochao Dun holds a Ph.D. in Physics from Wake Forest University and is currently a project scientist at Lawrence Berkeley National Laboratory. He specializes in entropy-driven materials design, hydrogen production and storage, and sustainable energy harvesting. His contributions include developing high-entropy materials for thermal catalysis, hydrogen-bonded organic-inorganic frameworks for critical mining recovery, and low-dimensional chalcogenides for thermoelectrics.

Xiaotian Zhang holds expertise on the large-scale growth of two-dimensional chalcogenide films through metalorganic chemical vapor deposition. He received his Ph.D. degree from the Pennsylvania State University, USA. He was also a key contributor to the 2D Crystal Consortium - Materials Innovation Platform. After his graduation, Dr. Zhang further extended his research endeavors at the Advanced Light Source of Lawrence Berkeley National Laboratory, USA. Presently, he holds the position of Assistant Professor at the School of Mechanical Engineering, Shanghai Jiao Tong University in China. His current research focuses on the synthesis and characterization of emerging functionalized two-dimensional thin films.

Zhiyu Hu, currently serving as the Zhi Yuan Chair Professor at Shanghai Jiao Tong University, holds the positions of National Chair Professor and Professor Class II. He is a Fellow of the Royal Society of Chemistry (FRSC). Additionally, he is the esteemed founder and director of the Institute of Nano/Micro Energy. With a wealth of experience, Zhiyu Hu's research focuses on NEMS- and MEMS-based devices, nanoscale energy conversion, nano-constructed functional materials, and nano-optics. His expertise in these areas stems from his past role as a research staff member at the Oak Ridge National Laboratory (ORNL) within the U.S. Department of Energy. Prior to his current position, he held the esteemed title of Distinguished Professor at Shanghai University.